ever, some relevant boundary-layer instability information is available.

Hot-wire anemometry experiments have provided many details of the major disturbances found in planar and conical laminar boundary layers and Ref. 6 contains some pertinent data at a Mach number of 8. These experiments demonstrated that the dominant disturbances in the laminar boundary layer on a sharp cone at zero angle of attack at Mach 8 were second-mode disturbances, the high frequency, acoustical-type disturbances identified by Mack's linear stability analyses.[8,9] Numerical results[10] for the laminar planar boundary layer indicated that second-mode disturbances should also be the major disturbances in the planar boundary layer. However, the hot-wire anemometry data demonstrated that this was not the case. The major disturbances were low-frequency disturbances that were growing in a frequency band that the linear stability analysis indicated should be stable.[6] These Mach 8 planar results appear similar to the flat-plate results obtained by Kendall[11] at Mach numbers of 3.0, 4.5, and 5.6. Kendall reported that "fluctuations of all frequencies were observed to grow monotonically larger in the region of a boundary layer extending from the flat-plate leading edge to the predicted location of instability; i.e., in a region where no growth was expected." This early growth of disturbances was attributed to the strong sound field generated by the turbulent boundary layer on the nozzle wall. Although stability theory predicts that the second-mode instability will be the primary instability at Mach numbers 4.5 and 5.6, Kendall found no evidence to indicate a dominating presence of second-mode waves. However, when testing with a cone model at $M_\infty = 8.5$ ($M_e = 7.7$), second-mode disturbances were the dominant disturbances. Thus, these data (Refs. 6 and 11) indicate that for planar boundary layers between Mach numbers 3 and 8, the major disturbances are low-frequency disturbances that are growing in a frequency band expected to be stable. This situation has never been observed in conical boundary layers.

It is interesting to note that cone transition data obtained in ballistic ranges[4,5] produced a unit-Reynolds-number slope even steeper than the wind-tunnel planar slope. Intuitively, it would seem that the different slopes of the transition Reynolds number vs the unit-Reynolds-number data was a significant point, but at this time one can only speculate as to the causes.

References

[1]Potter, J. L., and Whitfield, J. D., "Effects of Slight Nose Bluntness and Roughness on Boundary-Layer Transition in Supersonic Flows," *Journal of Fluid Mechanics*, Vol. 12, Pt. 4, 1962, pp. 501–535.

[2]Pate, S. R., "Measurements and Correlations of Transition Reynolds Numbers of Sharp Slender Cones at High Speeds," *AIAA Journal*, Vol. 9, No. 6, 1971, pp. 1082–1090.

[3]Morkovin, M. V., "Instability, Transition to Turbulence and Predictability," AGARDograph 236, July 1978.

[4]Potter, J. L., "Boundary-Layer Transition on Supersonic Cones in an Aeroballistic Range," *AIAA Journal*, Vol. 13, No. 3, 1975, pp. 270–277.

[5]Potter, J. L., "The Unit Reynolds Number Effect on Boundary-Layer Transition," Dissertation submitted in partial fulfillment of the requirements for the Degree of Doctor of Philosophy, Vanderbilt Univ., Nashville, TN, May 1974.

[6]Stetson, K. F., Kimmel, R. L., Thompson, E. R., Donaldson, J. C., and Siler, L. G., "A Comparison of Planar and Conical Boundary Layer Stability and Transition at a Mach Number of 8," AIAA Paper 91-1639, June 1991.

[7]Donaldson, J. C., private communication, Arnold AFB, TN Calspan Corp., Jan 1991.

[8]Mack, L. M., "Linear Stability Theory and the Problem of Supersonic Boundary-Layer Transition," *AIAA Journal*, Vol. 13, No. 3, 1975, pp. 278–289.

[9]Mack, L. M., "Boundary Layer Linear Stability Theory," AGARD Rept. No. 709, June 1986.

[10]Gasperas, G., "Effect of Wall Temperature Distribution on the Stability of Compressible Boundary Layer," AIAA Paper 89-1894, June 1989.

[11]Kendall, J. M., "Wind Tunnel Experiments Relating to Supersonic and Hypersonic Boundary Layer Transition," *AIAA Journal*, Vol. 13, No. 3, 1975, pp. 290–299.

Near-Wall Two-Equation Model for Compressible Turbulent Flows

H. S. Zhang* and R. M. C. So†
Arizona State University,
Tempe, Arizona 85287
C. G. Speziale‡
ICASE, NASA Langley Research Center,
Hampton, Virginia 23665
and
Y. G. Lai§
CFD Research Corporation,
Huntsville, Alabama 35801

Introduction

DIRECT numerical simulations of compressible turbulent flows, at high Reynolds numbers with all scales resolved, will probably not be possible in the foreseeable future, if ever at all. Therefore, turbulence modeling will continue to play a crucial role in the aerodynamic design of advanced aircraft. In high-speed aerodynamic applications, near-wall turbulence modeling is extremely important for the accurate prediction of crucial design parameters such as the skin friction and heat transfer coefficients. Despite its technological importance, progress in near-wall turbulence modeling has been slow. Many commonly used near-wall models, which contain a variety of ad hoc wall damping functions, are not asymptotically consistent and yield poor predictions even for simple incompressible boundary-layer flows.[1] These deficiencies can be fatal when turbulence models are applied to complex flows where it is necessary to integrate the governing equations directly to the wall. High-speed compressible flows present a whole range of new problems to near-wall turbulence modeling. Shock/boundary-layer interactions with turbulence amplification and flow separation represent but two examples. Two-dimensional equilibrium turbulent boundary layers are less of a problem provided that the external Mach number M_∞ is less than 5. For such flows, it can be argued that the turbulence statistics are only altered by compressibility effects through changes in the mean density—the crux of the Morkovin hypothesis[2] which allows for the use of variable density extensions of existing incompressible turbulence models where explicit dilatational terms are neglected. However, even the ability of these models to reliably predict mean flow properties in two-dimensional equilibrium boundary layers for $M_\infty \geq 5$ has been recently called into question.[3] For nonequilibrium compressible flows involving shocks and hypersonic speeds, the issue of near-wall turbulence modeling is even more unsettled.[4]

This Note makes an attempt to verify that asymptotically consistent near-wall modeling is crucial for the accurate prediction of high-speed compressible flows. This is accomplished by invoking Morkovin's hypothesis[2] in the extension of the recent near-wall k-ϵ model of So et al.[5] to compressible flows. The resulting compressible two-equation model is tested for boundary-layer flows with M_∞ as high as 10 and with wall cooling ratios T_w/T_{aw} as low as 0.3.

Received Dec. 18, 1991; presented as Paper 92-0442 at the AIAA 30th Aerospace Sciences Meeting, Reno, NV, Jan. 6-9, 1992; revision received May 27, 1992; accepted for publication May 30, 1992.

*Graduate Assistant, Mechanical and Aerospace Engineering.
†Professor, Mechanical and Aerospace Engineering. Member AIAA.
‡Senior Staff Scientist. Member AIAA.
§Scientist.

Two-Equation Turbulence Model

A detailed derivation of the compressible modeled equations to be considered herein has been given by Zhang et al.[6] In terms of the Favre-averaged equations of motion, this turbulence model can be summarized as follows:

$$\frac{\partial \bar{\rho}}{\partial t} + (\bar{\rho}\tilde{u}_i)_{,i} = 0 \tag{1}$$

$$\frac{\partial}{\partial t}(\bar{\rho}\tilde{u}_i) + \bar{\rho}\tilde{u}_i\tilde{u}_j)_{,j} = -\bar{p}_{,i} - \frac{2}{3}(\bar{\mu}\tilde{u}_{j,j})_{,i} + [\bar{\mu}(\tilde{u}_{i,j} + \tilde{u}_{j,i})]_{,j} - (\bar{\rho}\tau_{ij})_{,j} \tag{2}$$

$$\frac{\partial}{\partial t}(\bar{\rho}\tilde{C}_p\tilde{T}) + (\bar{\rho}\tilde{u}_i\tilde{C}_p\tilde{T})_{,i} = \frac{\partial \bar{p}}{\partial t} + \tilde{u}_i\bar{p}_{,i} + \overline{u_i''}\bar{p}_{,i} - \overline{p'u'_{i,i}} - (\bar{p}\overline{u_i''})_{,i} + (\bar{\rho}R\widetilde{u_i''T''})_{,i} + \bar{\sigma}_{ij}\tilde{u}_{i,j} + \bar{\sigma}_{ij}\overline{u_{i,j}''} + \bar{\rho}\epsilon - (\bar{\rho}\tilde{C}_p\widetilde{u_i''T''})_{,i} + (\bar{k}\widetilde{T}_{,i})_{,i} \tag{3}$$

$$\frac{\partial}{\partial t}(\bar{\rho}K) + (\bar{\rho}\tilde{u}_iK)_{,i} = -\bar{\rho}\tau_{ij}\tilde{u}_{i,j} - \bar{\rho}\epsilon_s + \left[\left(\bar{\mu} + \frac{\mu_T}{\sigma_k}\right)K_{,i}\right]_{,i} \tag{4}$$

$$\frac{\partial}{\partial t}(\bar{\rho}\epsilon_s) + (\bar{\rho}\tilde{u}_i\epsilon_s)_{,i} = -C_{\epsilon 1}\frac{\bar{\rho}\epsilon_s}{K}\tau_{ij}\tilde{u}_{i,j} - C_{\epsilon 2}f_2\bar{\rho}\frac{\epsilon_s^2}{K} + \left[\left(\bar{\mu} + \frac{\mu_T}{\sigma_\epsilon}\right)\epsilon_{s,i}\right]_{,i} \tag{5}$$

where

$$\bar{\sigma}_{ij} = -\frac{2}{3}\bar{\mu}\tilde{u}_{k,k}\delta_{ij} + \bar{\mu}(\tilde{u}_{i,j} + \tilde{u}_{j,i}) \tag{6a}$$

$$\tau_{ij} = \frac{2}{3}K\delta_{ij} - \mu_T\left(\tilde{u}_{i,j} + \tilde{u}_{j,i} - \frac{2}{3}\tilde{u}_{k,k}\delta_{ij}\right) \tag{6b}$$

$$\widetilde{u_i''T''} = -\frac{\mu_T}{\bar{\rho}Pr_T}\tilde{T}_{,i} \tag{7a}$$

$$\overline{u_i''} = \frac{\mu_T}{\bar{\rho}^2\sigma_\rho}\bar{\rho}_{,i} \tag{7b}$$

are the viscous stress, Reynolds stress, Reynolds heat flux, and mass flux, respectively. In these equations, an overbar and prime are used for the standard Reynolds decomposition whereas an overtilde and dourle prime are used for the Favre decomposition. The eddy viscosity is given by $\mu_T = \bar{\rho}C_\mu f_\mu K^2/\epsilon_s$ where $K = \tau_{ii}/2$ is the turbulent kinetic energy and ϵ_s is the solenoidal part of the turbulent dissipation rate. The compressible dissipation rate $\epsilon_c(\epsilon = \epsilon_s + \epsilon_c)$ and the pressure dilatation correlation $p'u'_{i,i}$ are neglected along with turbulent fluctuations in the viscosity μ and specific heat C_p. The ideal gas law $p = \rho RT$ is used where R is the ideal gas constant. The two wall damping functions f_μ and f_2 are variable density extensions of those proposed by So et al.[5]:

$$f_\mu = (1 + 3.45/\sqrt{R_t})\tanh[y^+/115] \tag{8a}$$

$$f_2 = \tilde{\epsilon}_s/\epsilon_s[1 + (2f_{w2}/C_{\epsilon 2}) - 3/2\,(f_{w2}/C_{\epsilon 2})(\epsilon_s^{*2}/\epsilon_s\tilde{\epsilon}_s)] \tag{8b}$$

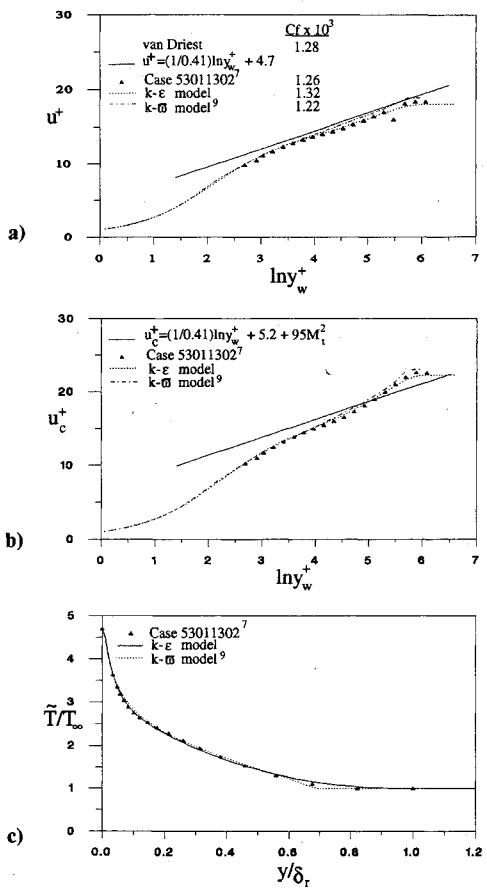

Fig. 1 Comparison of calculated and measured mean profiles for the $M_\infty = 4.544$, $T_w/T_{aw} = 1.0$ case: a) standard log-law plot of mean velocity; b) compressible law-of-the-wall plot; and c) linear plot of mean temperature.

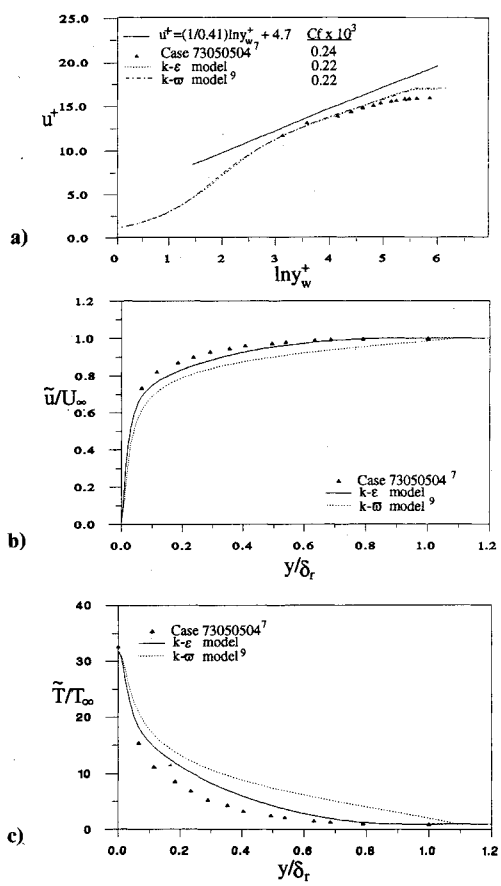

Fig. 2 Comparison of calculated and measured mean profiles for the $M_\infty = 10.31$, $T_w/T_{aw} = 1.0$ case: a) standard log-law plot of mean velocity; b) linear plot of mean velocity; and c) linear plot of mean temperature.

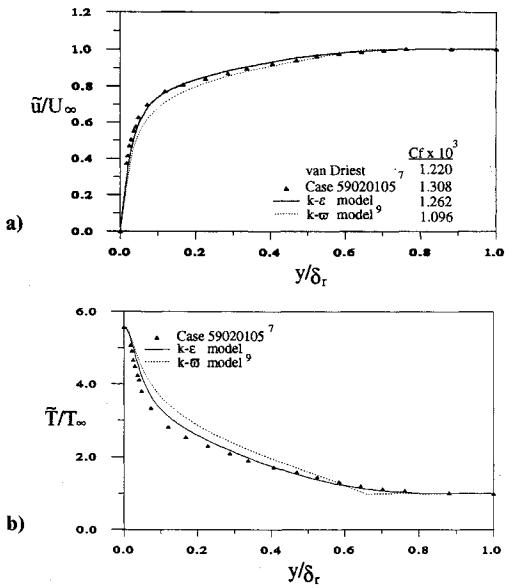

Fig. 3 Comparison of calculated and measured mean profiles for the $M_\infty = 5.29$, $T_w/T_{aw} = 0.92$ case: a) linear plot of mean velocity; and b) linear plot of mean temperature.

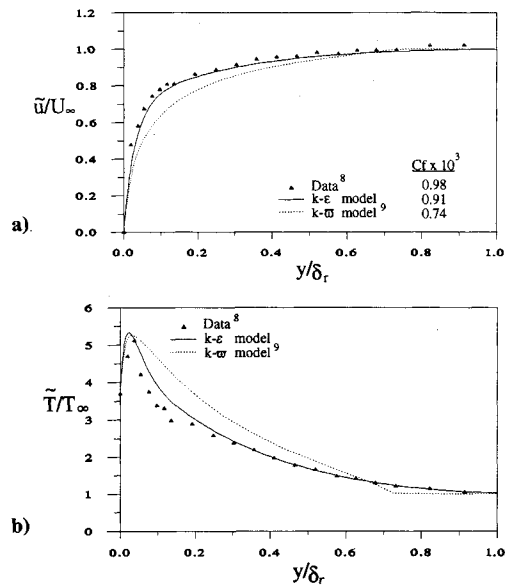

Fig. 4 Comparison of calculated and measured mean profiles for the $M_\infty = 8.18$, $T_w/T_{aw} = 0.3$ case: a) linear plot of mean velocity; and b) linear plot of mean temperature.

where $R_t = K^2/\bar{\nu}\epsilon_s$, $f_{w2} = \exp[-(R_t/64)^2]$, $\epsilon_s^* = \epsilon_s - 2\bar{\nu}K/y^2$, $\tilde{\epsilon}_s = \epsilon_s - 2\bar{\nu}(\sqrt{K})_{,i}(\sqrt{K})_{,i}$, $\bar{\nu} = \bar{\mu}/\bar{\rho}$, $u_\tau = \sqrt{\tau_w/\bar{\rho}_w}$, and $y^+ = yu_\tau/\bar{\nu}$. The model constants are $C_\mu = 0.096$, $C_{\epsilon 1} = 1.5$, $C_{\epsilon 2} = 1.83$, $\sigma_k = 0.75$, $\sigma_\epsilon = 1.45$, and $\sigma_\rho = 0.5$; the turbulent Prandtl number Pr_T is taken to be 0.9.

Discussion of Results

The k-ϵ model outlined in the preceding section is used to calculate compressible flat plate boundary layers on adiabatic and cooled walls. The calculations are carried out over the range, $0 < M_\infty < 10$, for the adiabatic wall boundary condition and over the range $0 < T_w/T_{aw} < 1$ for the constant cooled-wall temperature condition. Comparisons are made with the mean velocity and temperature profiles as well as with the reported skin-friction coefficient, $C_f = 2\tau_w/(\bar{\rho}_\infty U_\infty^2)$ drawn from Refs. 7 and 8. All calculations are carried out to the same momentum thickness Reynolds number R_θ as the measurements and the comparisons are made at these respective locations. Three sets of data are chosen from Ref. 7. These are cases 53011302 and 73050504 with an adiabatic wall and case 59020105 with $T_w/T_{aw} = 0.92$. M_∞ for these cases are 4.544, 10.31, and 5.29, respectively, and the corresponding R_θ are 5532, 15,074, and 3939. The fourth case with $M_\infty = 8.18$, $T_w/T_{aw} = 0.3$, and $R_\theta = 4600$ is selected from Ref. 8. The mean profiles are also compared with the k-ω calculations[9] and with van Driest's compressible law-of-the-wall.[10]

The results are plotted in Figs. 1-4 with each figure showing the comparisons for a fixed M_∞. The mean velocities are presented in two different forms; one in terms of wall variables, u^+ vs $\ell n\, y_w^+$, and another in terms of outer variables, $\tilde{u}/U_\infty$ vs y/δ_r. Here, $u^+ = \tilde{u}/u_\tau$, $y_w^+ = yu_\tau/\bar{\nu}_w$ and δ_r is the measured boundary-layer thickness. The mean temperature is plotted in the form of $\tilde{T}/T_\infty$ vs y/δ_r. Whenever possible, the calculated and measured C_f, plus that determined from the van Driest II formula,[10] are listed in the figures for comparison. A traditional and compressible law-of-the-wall are also shown for comparison in the figures. According to Ref. 10, the compressible van Driest coordinate is defined by

$$u_c^+ = \int_0^{u^+} (\bar{\rho}/\bar{\rho}_w)^{1/2} du^+$$

The log-law is seen to hold true for all cases calculated using both the k-ϵ and k-ω models (Figs. 1a,b and 2a) and the von Karman constant κ thus determined for the adiabatic wall cases is essentially 0.41. For the cooled-wall case, the calculated κ is not equal to 0.41 and varies from model to model. Therefore, the semilog plots are not shown in Figs. 3 and 4. All models considered yield calculations of C_f that are in agreement with measured data and with van Driest II values.[10] The maximum error in C_f predictions is less than 4% (Figs. 1a and 2a). Exceptions are the cooled-wall cases where the predictions are much lower than measurements but higher than van Driest II values (Figs. 3a and 4a). The velocity plots of u_c^+ vs $\ell n\, y_w^+$ for case 53011302 are compared with the compressible law-of-the-wall[10] in Fig. 1b. A line that is parallel to the compressible law-of-the-wall can be drawn through a few of the data points spanning over a narrow range of y_w^+. On the other hand, the calculated profiles are in agreement with data over a wider range of y_w^+ when plotted in the form u^+ vs $\ell n\, y_w^+$. The slopes of the calculated profiles are roughly parallel to that determined from measurements and are slightly larger than the slope of the compressible law-of-the-wall shown. Therefore, the slope of the log-law is given by 1/0.41 only when the profiles are plotted in terms of u^+. The present results show that there are substantial discrepancies between measurements and the profiles of $\tilde{u}/U_\infty$ and $\tilde{T}/T_\infty$ calculated using the k-ω model (Figs. 2b, 3a,b, and 4a,b). The discrepancies increase as M_∞ increases and as T_w/T_{aw} decreases. One reason is that, unlike the k-ϵ model, the k-ω calculated δ is smaller than δ_r for $M_\infty < 5$ and much larger than δ_r for $M_\infty = 10.31$ (Fig. 2b). The same can also be said of the cooled-wall cases (Figs. 3a and 4a), where large discrepancies exist between k-ω calculations and measurements, particularly for the case with $T_w/T_{aw} = 0.3$. On the other hand, the disagreement between k-ϵ calculations and measurements appear to be attributed to the assumption of a constant Pr_T. This can be remedied by the adoption of a variable Pr_T model.[11]

In conclusion, the present results definitively show that, contrary to recent speculations, a variable-density extension of an asymptotically sound two-equation model of the k-ϵ type can accurately predict compressible boundary layers, with a wide range of wall cooling ratios, for Mach numbers as large as ten.

Acknowledgments

Funding support to R. M. C. So from NASA Langley Research Center under Grant NAG1-1080 and to C. G. Speziale under Contract NAS1-18605, while in residence at ICASE, is gratefully acknowledged.

References

[1]Patel, V. C., Rodi, W., and Scheuerer, G., "Turbulence Models for Near-Wall and Low Reynolds Number Flows: A Review," *AIAA Journal*, Vol. 23, No. 9, 1985, pp. 1308–1319.

[2]Morkovin, M., "Effects of Compressibility on Turbulent Flows," *Mecanique de la Turbulence*, edited by A. Favre, Centre National de la Recherche Scientifique, Paris, 1962, pp. 367–380.

[3]Bradshaw, P., Launder, B. E., and Lumley, J. L., "Collaborative Testing of Turbulence Models," *Journal of Fluids Engineering*, Vol. 113, No. 1, 1991, pp. 3–4.

[4]Bushnell, D. M., "Turbulence Modeling in Aerodynamic Shear Flows," AIAA Paper 91-0214, Jan. 1991.

[5]So, R. M. C., Zhang, H. S., and Speziale, C. G., "Near-Wall Modeling of the Dissipation-Rate Equation," *AIAA Journal*, Vol. 29, No. 12, 1991, pp. 2069–2076.

[6]Zhang, H. S., So, R. M. C., Speziale, C. G., and Lai, Y. G., "A Near-Wall Two-Equation Model for Compressible Turbulent Flows," AIAA Paper 92-0442, Jan. 1992.

[7]Fernholz, H. H., and Finley, P. J., "A Critical Compilation of Compressible Turbulent Boundary Layer Data," AGARDograph No. 223, June 1977.

[8]Kussoy, M. I., and Horstman, K. C., "Documentation of Two- and Three- Dimensional Shock-Wave/Turbulent-Boundary-Layer Interaction Flows at Mach 8.2," NASA TM-103838, May 1991.

[9]Wilcox, D. C., "Reassessment of the Scale-Determining Equation for Advanced Turbulence Models," *AIAA Journal*, Vol. 26, No. 11, 1988, pp. 1299–1310.

[10]Bradshaw, P., "Compressible Turbulent Shear Layers," *Annual Review of Fluid Mechanics*, Vol. 9, 1977, pp. 33–54.

[11]Sommer, T. P., So, R. M. C., and Zhang, H. S., "Near-Wall Variable-Prandtl-Number Turbulence Model for Compressible Flows," *AIAA Journal*, Vol. 31, No. 1, pp. 27–35.

Nonparameterized 'Entropy Fix' for Roe's Method

François Dubois*
Aerospatiale Espace & Defense,
78133 Les Mureaux, France
and
Guillaume Mehlman†
Ecole Polytechnique,
Centre de Mathématiques Appliquées,
91128 Palaiseau, France

Introduction

ROE'S approximate Riemann solver is very popular and enables easy upwinding for general computational fluid dynamics (CFD) problems. The main drawback with this method is that nonphysical expansion shocks can occur in the vicinity of sonic points. We recall that Roe's method[1] for the general hyperbolic system of conservation laws

$$\frac{\partial U}{\partial t}+\frac{\partial F(U)}{\partial x}=0 \tag{1}$$

consists in replacing the exact solution of local Riemann problems by the solution of the approximate linear hyperbolic problem whose flux function is defined by

$$F(U_k,\ U_{k+1},\ U)=F(U_k)+A(U_k,U_{k+1})\cdot(U-U_k)$$

between the grid points U_k and U_{k+1}. The matrix $A(U_l,\ U_r)$ is called a Roe-type linearization and is required to have the following properties:

1) $F(U_r)-F(U_l)=A(U_l,\ U_r)\cdot(U_r-U_l)$
2) $A(U,U)=\mathrm{d}F(U)$
3) $A(U_l,U_r)$ has real eigenvalues and a complete set of eigenvectors.

In the sequel, we assume that system (1) is hyperbolic and admits a Roe-type linearization. We also assume that U is an m-column vector and that the flux function $F(U)$ is a vector-valued function of m components. Let $r_i(U)$ and $\lambda_i(U)$ denote the eigenvectors and associated eigenvalues of the jacobian $\mathrm{d}F(U)$. Similarly, let $R_i(U_l,U_r)$ and λ_i^R denote the eigenvectors and associated eigenvalues of the matrix $A(U_l,U_r)$.

There are several objections to the spreading devices classically used[2,3] in order to cope with nonphysical solutions. In both previous examples, the underlying idea is to give an a priori representation of the solution. We present a new approach based on a nonlinear modification of the flux function.

Definition of the Modified Flux Function

Since problems occur at sonic points, we decide to modify F^R only at sonic points. Let w_j denote the characteristic variables

$$U-U_l=\sum_{j=1}^{m}w_jR_j(U_l,U_r)$$

In particular, we designate by α_j the characteristic variables associated with the jump U_r-U_l. We define m intermediate states:

$$U_0=U_l\ ,\ \ldots\ ,\ U_j=U_{j-1}+\alpha_jR_j(U_l,U_r)\ ,\ \ldots\ ,\ U_m=U_r$$

Let S be the set of sonic indices

$$S=\{j,\ \lambda_j(U_{j-1})<0<\lambda_j(U_j)\}$$

We introduce the following modified flux function parameterized by U_l and U_r:

$$F^{DM}(U_l,U_r,U)=F(U_l)+\sum_{i=1}^{m}g_i(w_i)R_i(U_l,U_r)$$

where the g_is are parameterized by the states $(U)_{j=1,\ldots,m}$ and are defined for $\alpha_i>0$ according to

$$\text{if}\quad i\notin S,\quad \forall w,\quad g_i(w)=\lambda_i^R\cdot w$$

$$\text{if}\quad i\in S,\quad g_i(w)=\begin{cases}p_i(w), & 0<w<\alpha_i\\ \lambda_i^R\cdot w, & w<0 \text{ or } w>\alpha_i\end{cases}$$

and where p_i is the unique Hermite polynomial of degree 3 defined by the conditions:

$$g_i(0)=0,\quad g_i(\alpha_i)=\lambda_i^R\cdot\alpha_i,\quad g_i'(0)=\lambda_i(U_{i-1}),\quad g_i'(\alpha_i)=\lambda_i(U_i)$$

Note that $\lambda_i(U_{i-1})$ and $\lambda_i(U_i)$ are the true eigenvalues of the physical flux at the intermediate states U_i given by the Roe-matrix $A(U_l,U_r)$. Away from sonic points, F^{DM} coincides with the linearized Roe flux F^R. If the initial flux F in Eq. (1) is at least of class C^1, and if the matrix $A(U_l,U_r)$ is continuous with respect to U_l and U_r, then the modified flux F^{DM} is a continuous function of all three arguments.

Definition of the Modified Numerical Flux

Let $V_{l,r}$ be the unique entropy solution of the Riemann problem

$$\begin{cases}\dfrac{\partial V}{\partial t}+\dfrac{\partial F^{DM}(U_l,\ U_r,\ V)}{\partial x}=0\\ V(x,0)=\begin{cases}0, & x<0\\ U_r-U_l, & x>0\end{cases}\end{cases}$$

Received June 13, 1991; presented at the AIAA 10th Computational Fluid Dynamics Conference, Honolulu, HI, June 24–27, 1991; revision received Sept. 6, 1991; accepted for publication Sept. 12, 1991.

*Chief, Département Mathématiques Appliquées et Calcul Scientifique. Member AIAA.

†Research Scientist. Member AIAA.